Dynamics of a Fixed-Bed Adsorptive Reactor for Synthesis of Diethylacetal

Viviana M.T.M. Silva and Alírio E. Rodrigues
Laboratory of Separation and Reaction Engineering, Faculdade de Engenharia da Universidade do Porto, 4200-465 Porto, Portugal

Diethylacetal from ethanol and acetaldehyde catalyzed by the acid resin Amberlyst 18 was synthesized. Adsorption and reaction experiments were performed in a laboratory-scale fixed-bed adsorptive reactor, operating isothermally at 15°C and at atmospheric pressure. Experimental results of dynamic adsorption of binary nonreactive mixtures were used to obtain multicomponent adsorption equilibrium isotherms of the Langmuir type. The reaction kinetics reported earlier were used in the model of the adsorptive reactor, which also included axial dispersion, external and internal mass-transfer resistances, and multicomponent Langmuir isotherms. Model equations were solved by orthogonal collocation on finite elements (OCFE), implemented by the PDECOL package, using the measured model parameters, and were validated by experimental data for reaction and regeneration steps, with good accuracy.

Introduction

Acetals are oxygenated organic compounds used as starting materials for perfumes, agricultural chemicals, and pharmaceuticals (Iwasaki et al., 1996), and they are represented by the following structure: R_1—O—C (R_2) (R_3)—O—R_1, where R_1 is an alkyl group, and R_2 and R_3 each represent a hydrogen atom or an alkyl group.

Diethylacetal (herein called acetal) is an important raw material for fragrances and pharmaceutical products (Kaufhold and El-Chabawi, 1996) and is used in the flavoring of alcoholic drinks (Kelly et al., 1999). In perfumery, acetal is used for the design of synthetic perfumes to increase the resistance to oxidation and therefore the lifetime of perfumes. Acetal is also widely used as an intermediate for the synthesis of various industrial chemicals, especially alkyl vinyl ethers and polyacetal resins (Aizawa et al., 1994).

In the past few years, the development of more environmentally acceptable gasolines and fuels has been studied intensively. Acetals have been under consideration as oxygenated additives to diesel fuel because they reduce drastically the emission of particles and NO_x (Thüner et al., 1999). Diethylacetal is used as an additive for ethanol fuel to decrease the auto ignition temperature (Kohlpaintner et al., 1999). Recently, it has been reported that it can make an attractive additive to diesel oil by keeping or improving the cetane number and helping in the combustion of the final products, without decreasing the ignition quality (Capeletti et al., 2000; Balzano and Laborde, 2000).

Most known methods of acetal production involve the acid-catalyzed equilibrium-controlled reaction of acetaldehyde and ethanol (Bramwyche et al., 1950), according to the reaction

$$2\ \text{Ethanol (A)} + \text{Acetaldehyde (B)} \leftrightarrows \text{Acetal (C)} + \text{Water (D)}.$$

Traditionally, mineral or carboxylic acids are used as the catalyst (Morrison and Boyd, 1983). The disadvantage of using soluble catalysts is that they must be neutralized after reaction. Therefore, heterogeneous catalysts of the strongly acid resin type are used. These catalysts have the advantage of being easily separated from the reaction product and having a long lifetime. Resins are of particular interest, since they act like a catalyst for the acetalization reaction and as a selective adsorbent to the species involved in the process (Mazzotti et al., 1996, 1997). Lately, the development of multifunctional reactors using acid resins as the catalyst is being implemented in the production of oxygenated fuel additives

Correspondence concerning this article should be addressed to A. E. Rodrigues.

(MTBE, ETBE, TAME, and so on), where the reaction is of the type: $A + B \leftrightarrows C$. Among all available technologies, the reactive distillation is the most used in that field, since differences between the boiling points of reactants, A and B, and the desired product, C, are sufficient (Sundmacker and Hoffman, 1996; Higler et al., 2000). In the case of acetalization, where the two products, acetal and water, have boiling temperatures of 102°C and 100°C, respectively, the use of an adsorptive/chromatographic reactor seems to be a feasible and economical solution. The application of chromatographic reactors to equilibrium-controlled reactions (Sardin et al., 1992; Carta, 1990) leads to conversions that are higher than the equilibrium, since one of the products is being removed from the reaction zone. Perhaps one of the most interesting chromatographic reactors is the simulated moving-bed reactor (SMBR). This technology has been applied to reversible reactions catalyzed by acid resins (Kawase et al., 1996; Mazzoti et al., 1996) and also to biochemical reactions (Azevedo and Rodrigues, 2001; Barker et al., 1992). However, some authors first studied the dynamic behavior of the fixed-bed adsorptive reactor to validate kinetic and adsorption data and to provide a better understanding of the performance of chromatographic reactors (Lode et al., 2001; Mazzotti et al., 1997; Kawase et al., 1999).

The aim of this work is to study the synthesis of diethylacetal in a fixed-bed adsorptive reactor, in view of the future implementation of the process in a simulated moving-bed adsorptive reactor. Adsorption and reaction experiments were carried out at 288 K. The multicomponent adsorption parameters were obtained by performing binary adsorptive experiments in the absence of reaction. The reaction kinetics of acetal production, catalyzed by the sulfonic acid ion-exchange resin Amberlyst 18, obtained in a batch reactor by Silva and Rodrigues (2001), was considered. The model for the adsorptive reactor includes axial dispersion, external and internal mass-transfer resistances, constant temperature, and multicomponent Langmuir isotherms, and was solved by orthogonal collocation by finite elements, using the measured model parameters.

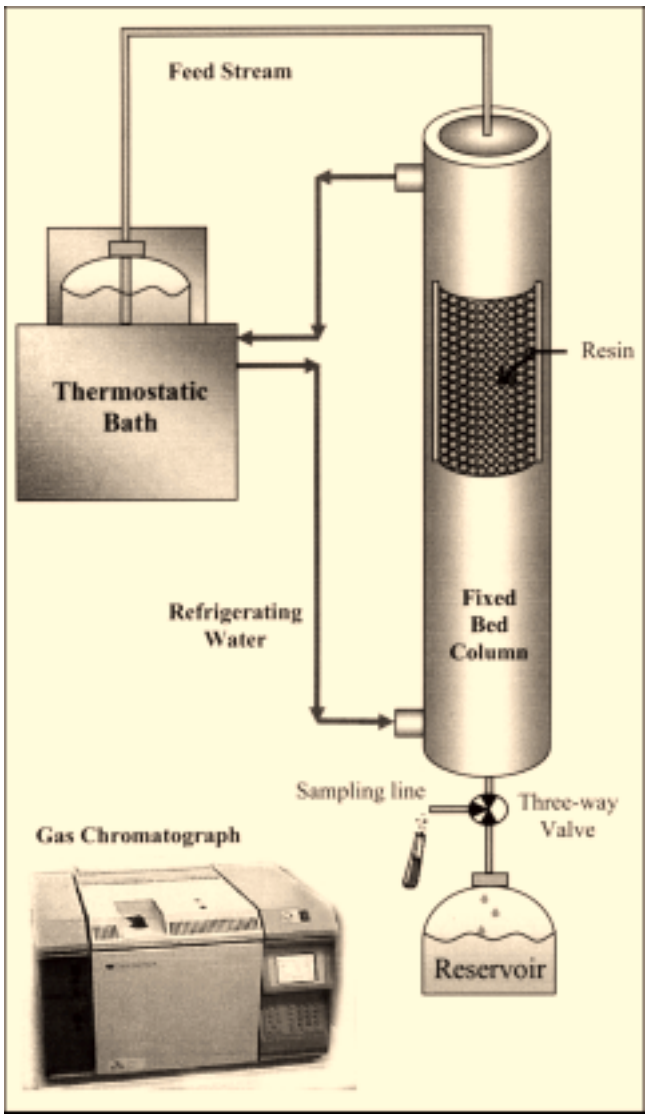

Figure 1. Experimental setup (configuration: top-down flow direction).

The Chromatographic Reactor

Experimental apparatus

The experiments have been performed in a laboratory-scale jacketed glass column that was maintained at constant temperature, through a thermostatic bath at 288 K, at atmospheric pressure (see Figure 1). All experiments were performed with analytical-grade chemicals (purity > 99%) from Sigma-Aldrich (U.K.). The experimental breakthrough curves were obtained by analyzing, with a gas chromatograph, small samples withdrawn at different times from the column exit. The column was packed with the sulfonic acid ion-exchange resin Amberlyst 18 (Rohm and Haas). The ion-exchange capacity is 4.5 eq $H^{\oplus}$/kg of dry resin and the inner surface area is 30×10^3 m^2/kg. When the dry resin contacts a fluid, it swells, and the swelling ratio (ratio between the swollen and dry volume of the resin) depends upon the fluid composition. The swelling is due to the sorption of the different components of the mixture, depending on their relative affinities to the resin. The character of the resin is mainly determined by its structure, for example, cross-linking degree and functional groups. The polymeric resins that contain sulfonic acid functional groups, such as Amberlyst 18, exhibit a strong selectivity for polar species. For Amberlyst 15 the swelling ratio for water, ethanol, acetic acid, and ethyl acetate is, respectively, 1.52, 1.48, 1.30, and 1.22 (Mazzotti et al., 1997), which is in agreement with the polarity of the components. Thus, it is expected for the system studied here that the order of increasing affinity of the components to the resin is acetal, ethanol, acetaldehyde, and water. The effect of swelling yields changes in the length and in the bulk porosity of the fixed-bed reactor, but during its operation no variations in the bed length were noticed. Table 1 shows the characteristics of the fixed-bed column.

In order to determine the Peclet number and the bed porosity, pulse experiments of the tracer were performed using a blue dextran solution (5 kg/m^3). Samples of 0.2 cm^3 were injected under different flow rates and the column responses were monitored using a UV-VIS detector at 300 nm.

Table 1. Characteristics of the Fixed-Bed Column

Solid weight	46×10^{-3} kg
Length (L)	28×10^{-2} m
Internal diameter	2.2×10^{-2} m
Radius of the particle (r_p)	239×10^{-6} m
External void fraction (ϵ)	0.39
Internal void fraction (ϵ_p)	0.39
Bulk density (ρ_b)	390 kg/m^3

The bed porosity was calculated from the stoichiometric time of the obtained experimental curves. By calculating the second moment of the experimental curves, an average Peclet number was obtained for the range of flow rates to be used in the fixed-bed experiments. Figure 2 shows two different tracer experiments and the respective values of bed porosity and Peclet number are presented in Table 2.

Mathematical model

A rigorous modeling of the sorption in the swelling polymer should include an appropriate model, such as the modified Flory–Huggins model, to predict the polymer-phase activities (Mazzotti et al., 1996). However, for densely cross-linked resins bearing highly polar groups on almost every monomer, these effects are poorly understood and this model should be regarded as an empirical tool to correlate the equilibrium data sorption and to predict the behavior of multicomponent mixtures (Lode et al., 2001). For this reason, an alternative approach based on the multicomponent Langmuir model was considered

$$q_i = \frac{Q_i K_i C_i}{1 + \sum_{j=1}^{n} K_j C_j}, \tag{1}$$

where Q_i and k_i represent the total molar capacity per unit volume of resin and the equilibrium constant for component i, respectively. It was shown that thermodynamic consistency

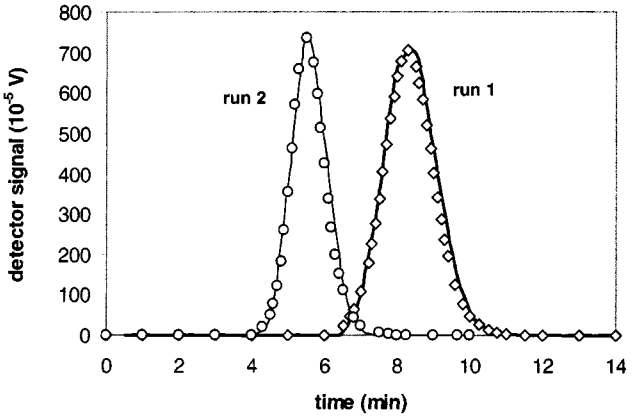

Figure 2. Tracer experiments, using a blue dextran solution.

Experimental results: (◇) run 1; (○) run 2. Simulated results: (——) run 1; (——) run 2.

Table 2. Results Obtained from Tracer Experiments

	Q ($\times10^7$ m^3/s)	τ (s)	ϵ	σ^2	Pe
Run 1	0.83	500	0.392	0.506	273.8
Run 2	1.25	335	0.393	0.234	265.7

requires that the total molar capacity of the resin should be equal for all species. For physical adsorption of molecules of widely different size such an assumption is unrealistic. Pöpken et al. (2000) states that using a Langmuir-type adsorption isotherm based on mass instead of adsorbed amount, where the total adsorbed mass per mass of catalyst was kept the same for all species, results in further improvement of the fitting result. It should also be mentioned that the underlying assumptions of the Langmuir model, that is, the monolayer adsorption to energetically equal binding sites, do not describe the actual physical phenomena of adsorption. However, the Langmuir model should be regarded as an analytical description rather than a physical model that is able to represent satisfactorily the experimental adsorption data.

The mathematical model used to describe the dynamic behavior of the fixed-bed adsorber/reactor considers the following assumptions:

(1) The flow pattern is described by the axial dispersed plug-flow model (Chung and Wen, 1968);

(2) External and internal mass-transfer for adsorbable species are combined in a global resistance;

(3) Isothermal process;

(4) Constant column length and packing porosity are assumed.

The model equations are constituted by the following system of four second-order partial differential equations in the bulk concentration of the ith component, C_i, and four ordinary differential equations in the average concentration of the ith component into the particle pores, $\overline{C}_{p,i}$

Bulk Fluid Mass Balance to Component i

$$\epsilon\frac{\partial C_i}{\partial t} + \frac{\partial (uC_i)}{\partial z} + (1-\epsilon)\frac{3}{r_p}K_L\left(C_i - \overline{C}_{p,i}\right) = \epsilon D_{\text{ax}}\frac{\partial}{\partial z}\left(C_T\frac{\partial x_i}{\partial z}\right). \tag{2}$$

Pellet Mass Balance to Component i

$$\frac{3}{r_p}K_L\left(C_i - \overline{C}_{p,i}\right) = \epsilon_p\frac{\partial \overline{C}_{p,i}}{\partial t} + \left(1-\epsilon_p\right)\frac{\partial q_i}{\partial t} - \nu_i\frac{\rho_b}{1-\epsilon}\Re^p, \tag{3}$$

together with the initial and Danckwerts boundary conditions

$$t = 0 \qquad C_i = \overline{C}_{p,i} = C_{i,0} \tag{4}$$

$$z = 0 \qquad uC_i - \epsilon D_{\text{ax}}\left.\frac{\partial C_i}{\partial z}\right|_{z=0} = uC_{i,F} \tag{5a}$$

$$z = L \qquad \left.\frac{\partial C_i}{\partial z}\right|_{z=L} = 0. \tag{5b}$$

The subscripts F and 0 refer to the feed and initial states, respectively, u is the superficial velocity, K_L is the global

Table 3. Reaction Equilibrium Constant and Kinetic Parameters of Acetal Synthesis Catalyzed by Amberlyst 18

T (K)	K_{eq}	k_c (mol/kg·s)	K_I
283	1.39	2.83	2.34
288	1.29	4.05	2.68

Source: Silva and Rodrigues (2001).

mass-transfer coefficient, D_{ax} is the axial dispersion coefficient, t is the time variable, z is the axial coordinate, ν_i is the stoichiometric coefficient of component i, ρ_b is the bulk density, and $\Re^p$ is the rate of the chemical reaction given by (Silva and Rodrigues, 2001):

$$\Re^p = k_c \frac{a_A a_B - a_C a_D / K_{eq} a_A}{\left(1 + K_I a_C / a_A\right)^2}, \tag{6}$$

where the activities of the components are relative to the liquid phase inside the catalyst pores. The activity coefficients were evaluated using the UNIFAC method (Fredenslund et al., 1977). The equilibrium constant and the kinetic parameters of Amberlyst 18 are presented in Table 3.

Variations in the superficial velocity and in the total concentration of the liquid phase can be accounted for by assuming the ideal volume additivity of the components within the liquid phase, that is, $\Sigma C_i V_{ml,i} = 1$. However, velocity and total concentration variations in the simulations under examination are small and can be neglected without significantly affecting the model accuracy.

Introducing the dimensionless variables for space $\zeta = z/L$ and time $\theta = t/(\epsilon L/u)$ and the parameters

$$Pe = \frac{uL}{\epsilon D_{ax}} \quad \text{(Peclet number)} \tag{7}$$

$$Da = \frac{\rho_b k_c \epsilon L}{(1-\epsilon)u} \quad \text{(Damköhler number)} \tag{8}$$

$$K_L^* = \frac{\epsilon L}{u}\frac{3}{r_p}k_L \quad \text{(Number of mass-transfer units)}. \tag{9}$$

The model Eqs. 2 and 3 become

$$\frac{\partial C_i}{\partial \theta} + \frac{\partial C_i}{\partial \zeta} + K_L^* \frac{1-\epsilon}{\epsilon}\left(C_i - \overline{C}_{p,i}\right) = \frac{1}{Pe}\frac{\partial^2 C_i}{\partial \zeta^2} \tag{10}$$

$$K_L^*\left(C_i - \overline{C}_{p,i}\right) = \epsilon_p \frac{\partial \overline{C}_{p,i}}{\partial \theta} + \left(1-\epsilon_p\right)\frac{\partial q_i}{\partial \theta} - \nu_i Daf\left(\overline{C}_{p,i}\right), \tag{11}$$

with the initial and boundary conditions

$$\theta = 0 \quad C_i = \overline{C}_{p,i} = C_{i,0} \tag{12}$$

$$\zeta = 0 \quad C_i - \frac{1}{Pe}\frac{\partial C_i}{\partial \zeta}\bigg|_{\zeta=0} = C_{i,F} \tag{13a}$$

$$\zeta = 1 \quad \frac{\partial C_i}{\partial \zeta}\bigg|_{\zeta=1} = 0. \tag{13b}$$

The proposed model considers a global mass-transfer coefficient (K_L) defined as

$$\frac{1}{K_L} = \frac{1}{k_e} + \frac{1}{\epsilon_p k_i}, \tag{14}$$

wherein k_e and k_i are, respectively, the external and internal mass-transfer coefficients to the liquid phase.

Santacesaria et al. (1982) showed that the internal mass-transfer coefficient varies in time, and the calculation of the rigorous value requires the solution of the complete model equations inside particles. As an approximation, the mean value estimated by Eq. 15 (Glueckauf, 1955) was used

$$k_i = \frac{5 D_m/\tau}{r_p}. \tag{15}$$

The external mass-transfer coefficient was estimated by the Wilson and Geankoplis correlation (Ruthven, 1984)

$$Sh_p = \frac{1.09}{\epsilon}\left(Re_p Sc\right)^{0.33} \quad 0.0015 < Re_p < 55, \tag{16}$$

where Sh_p and Re_p are, respectively, the Sherwood and Reynolds numbers, relative to particle

$$Sh_p = \frac{k_e d_p}{D_m} \tag{17}$$

$$Re_p = \frac{\rho d_p u}{\mu}, \tag{18}$$

and Sc is the Schmidt number

$$Sc = \frac{\mu}{\rho D_m}. \tag{19}$$

The diffusivities in multicomponent liquid mixture were estimated by the modified Wilke–Chang equation, proposed by Perkins and Geankoplis (Reid et al., 1987)

$$D_{Am} = 7.4 \times 10^{-8}\frac{(\phi M)^{1/2} T}{\mu V_{ml,A}^{0.6}} \tag{20}$$

$$\phi M = \sum_{\substack{j=1 \\ j \neq A}}^{n} x_i \phi_j M_j \tag{21}$$

where D_{Am} is the diffusion coefficient for a dilute solute A into a mixture of n components; T is the temperature; $V_{ml,A}$ is the molar volume of the solute A; x_j is the molar fraction for component j; ϕ_j is the association factor for component j, that is, equal to 2.6 for water, 1.5 for ethanol, and 1.0 for unassociated components. The mixture viscosity, μ, was pre-

dicted by the generalized corresponding states method purposed by Teja and Rice (1981).

The system of partial differential equations represented by Eqs. 10 to 13 is solved by the method of the lines (MOL) using orthogonal collocation in finite elements, with B-splines as base functions through numerical package PDECOL (Madsen and Sincovec, 1979). Fifty subintervals for spatial discretization along the z-axis were used, with two internal collocation points in each subinterval, resulting in 200–400 time-dependent ordinary differential equations for adsorption/reaction simulations. For all simulations there was a fixed tolerance value EPS equal to 10^{-7}.

Results and Discussion

Binary adsorption experiments

The breakthrough curves of ethanol, acetal, and water were measured in the absence of reaction. The resin was saturated with a certain component, A, after which the feed concentration of component B was changed stepwise. The adsorption parameters were optimized by minimizing the difference between experimental and simulated stoichiometric times of the breakthrough curves

$$t_{st} = \frac{L}{u}\left[\epsilon + (1-\epsilon)\epsilon_p + (1-\epsilon)(1-\epsilon_p)\frac{\Delta q}{\Delta C}\right], \quad (22)$$

where

$$\frac{\Delta q}{\Delta C} = \frac{q(C_F) - q(C_0)}{C_F - C_0}. \quad (23)$$

Then the mass-transfer parameters were estimated from the preceding equations, after the tortuosity was optimized from the experimental data by "best fit" procedure. For all simulations, the viscosity mixture and the diffusivity of each component in the liquid mixture were calculated at each time and any axial position, and so the mass-transfer parameters also depend on the liquid composition.

It should be noted that the hydrodynamic regime has an important effect on the experimental results, and the difference in densities of the species (see Table 4) can lead to axial backmixing driven by natural convection. The concentration fronts moving within the column are hydrodynamically stable if the component in the component above the front is less dense than the component under the front. In order to obtain reproducibility in the experimental results, the correct flow direction (bottom-up or top-down) has to be chosen. As an example, for a breakthrough experiment where acetal is fed to a column initially saturated with ethanol, the liquid flow direction must be bottom-up, due to the higher density of acetal as compared to the ethanol, as shown in Figure 3. So, the correct liquid flow direction was considered in all experiments performed.

Table 4. Adsorption Equilibrium Isotherms and Component Densities at 288 K

Component	Q ($\times 10^{-3}$ mol/m$^3_{res}$)	k ($\times 10^6$/m^3/mol)	ρ (kg/m^3)
Ethanol	25.9	195	795
Acetaldehyde	35.4	173	784
Acetal	15.9	71	836
Water	60.7	310	1003

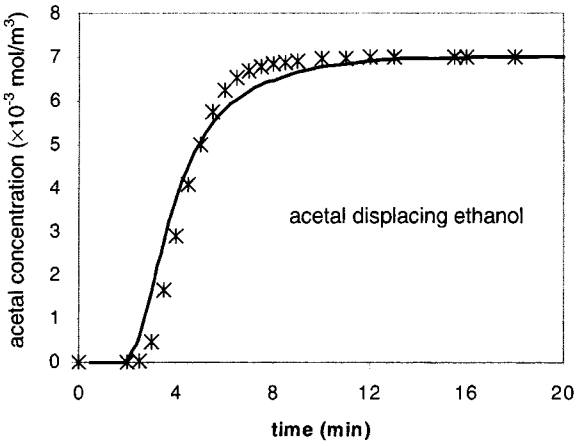

Figure 3. Breakthrough experiments: outlet concentration of acetal as a function of time.

Acetal displacing ethanol: $Q = 3.9 \times 10^{-7}$ m^3/s (23.2 mL/min); botton-up direction flow. (∗) Experimental acetal concentration; (——) model results.

In order to compare the selectivity of the resin to the components, two different experiments performed in the fixed-bed column are illustrated in Figure 4a and 4b; in both cases, top-down flow was used. In Figure 4a, ethanol displaces water, which initially saturates the resin. Since the resin preferentially adsorbs water, the concentration front of ethanol has a dispersive character. In Figure 4b, ethanol displaces acetal, which is the weakest adsorbed component, and in this case the breakthrough front of ethanol is self-sharpening.

In a breakthrough experiment, where component A displaces the component B, the total amount of A necessary to saturate the column is given by the product between the volumetric flow rate and the area over the breakthrough curve limited by the feed concentration. The product between the flow rate and the area under the elution curve gives the total amount of component B that was initially saturating the column. In Figure 5a and 5b, the concentration history of ethanol and water are shown. In the breakthrough of ethanol (Figure 5a), the errors between the experimental and simulated amounts of ethanol fed and water displaced are 1.2 and 0.5%, respectively. Comparing the amount of ethanol fed in the experiment of Figure 5b with the amount of ethanol displaced by water in the experiment of Figure 5a, the error obtained is 2.0%. For water, the error between the amount fed, Figure 5a, and the amount eluted, Figure 5b, is 2.0%.

It was not possible to perform the breakthrough experiments with acetaldehyde, because acetaldehyde reacts with itself to give an acetaldehyde trimer (paraldehyde). So the adsorption parameters were determined by optimization of the reaction data.

Kinetic experiments

In a typical reaction experiment, a mixture of ethanol and acetaldehyde is continuously fed to the chromatographic re-

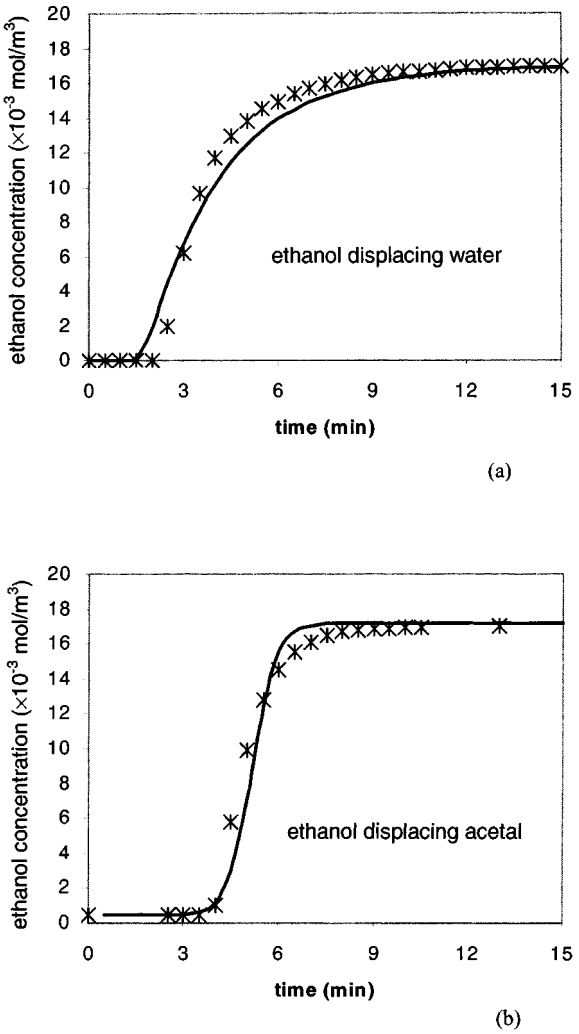

Figure 4. Breakthrough experiments: outlet concentration of ethanol as a function of time.

(a) Ethanol displacing water; $Q = 3.8 \times 10^{-7}$ m^3/s (23.0 mL/min); top-down direction flow; (b) ethanol displacing acetal; $Q = 3.6 \times 10^{-7}$ m^3/s (21.4 mL/min); top-down direction flow. (*) Experimental ethanol concentration; (——) model results.

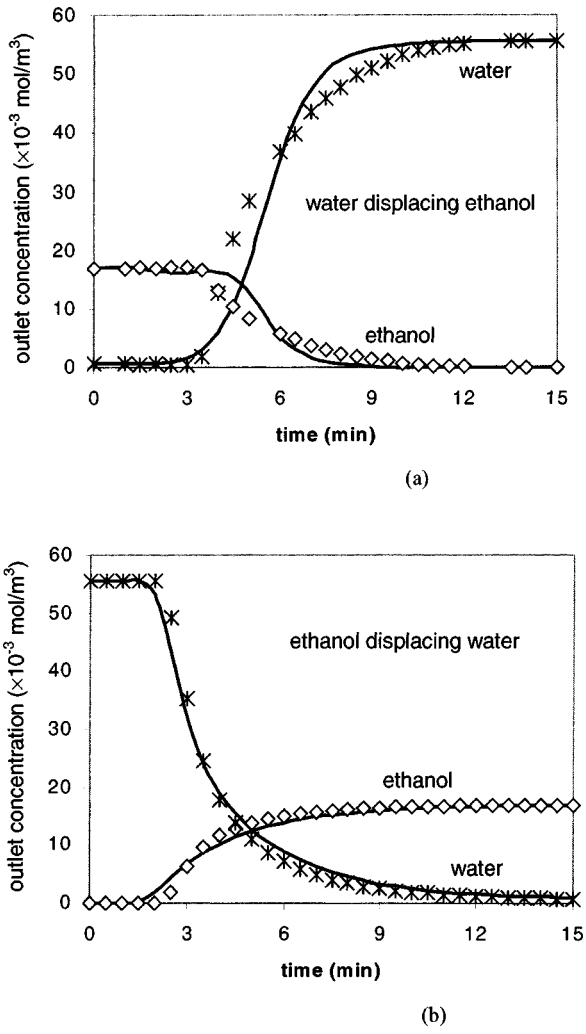

Figure 5. Breakthrough experiments: outlet concentration of ethanol and water as a function of time.

(a) Water displacing ethanol; $Q = 2.8 \times 10^{-7}$ m^3/s (16.7 mL/min); bottom-up direction flow; (b) ethanol displacing water; $Q = 3.9 \times 10^{-7}$ m^3/s (23.5 mL/min); top-down direction flow. Experimental data: (◇) ethanol; (∗) water; (——) model results.

actor, initially saturated with ethanol. Since the feed mixture is less dense than ethanol, the flow direction adopted was from the top to the bottom of the column. In the regeneration experiment, ethanol was used as desorbent and the top-down flow was adopted, because the reaction mixture present within the column is heavier than pure ethanol.

Two reaction experiments, where the feed is a mixture of ethanol and acetaldehyde that is almost at the stoichiometric ratio to a column initially saturated with ethanol, are shown in Figure 6, which shows the time evolution of the outlet concentrations. As the acetaldehyde enters the column, it is adsorbed and reacts with the adsorbed ethanol, in the resin phase. Acetal and water are formed in stoichiometric amounts, but the resin preferentially adsorbs water, whereas acetal is soon desorbed and carried by the fluid stream along the column. Since one of the products is removed from the reaction medium, the acetalization continues until the acetaldehyde is consumed. This process continues until the resin is completely saturated with acetaldehyde and water. When the resin reaches equilibrium, sorption, the selective separation of acetal and water, is not possible anymore. Local compositions remain constant, the steady state is achieved, and a reactive mixture at the equilibrium composition constitutes the outlet stream. The difference under the outlet concentration curves of the two products is relative to the difference in the adsorbed amount of acetal and water in the resin, once both products are formed at the same stoichiometric amount. In this case, the model predictions are quite good.

It is interesting to note that there are two concentration fronts. The first one is a separative front of acetal and ethanol, which occurs between 4 and 11 min (Figure 6). The second front is a reactive front where acetalization and separation of the products occur, and it is apparent after 12 min. These phenomena are better understood with the analysis of propa-

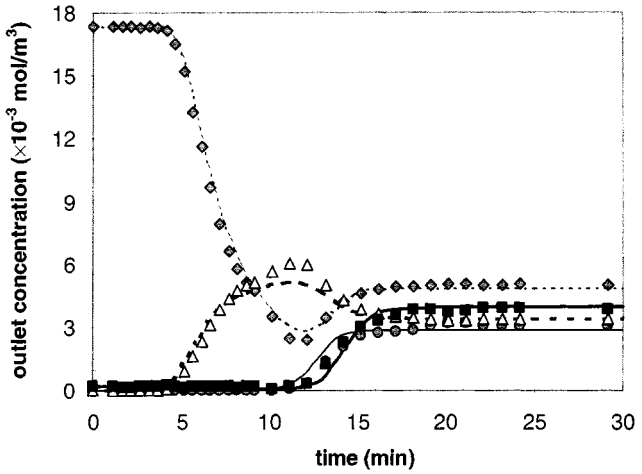

Figure 6. Concentration histories in a fixed-bed adsorptive reactor initially saturated with ethanol and then fed with ethanol and acetaldehyde.

Experimental conditions: $Q = 2.4 \times 10^{-7}$ m^3/s (14.5 mL/min), $C_{A0} = 11.7 \times 10^3$ mol/m^3 and $C_{B0} = 6.3 \times 10^3$ mol/m^3. Experimental data: (♦) ethanol; (●) acetaldehyde; (△) acetal; (■) water. Model results: (– – –) ethanol; (——) acetaldehyde; (– – –) acetal; (——) water.

gation of these composition fronts. This is only possible by considering the simulated profiles in the same experimental operating conditions of Figure 6. Figures 7a–7d show concentration profiles for each species at 1, 3, 6, and 9 min. At the entrance of the reactor, there is a reaction zone even when the steady state is reached. This reaction zone corresponds to the consumption of the acetaldehyde until the equilibrium composition ($C = 2.9 \times 10^3$ mol/m^3). When the equilibrium conversion is reached (at $\zeta = 0.25$ and $t > 180$ s, in Figure 7), the reactants' concentrations do not change until a second transition occurs. This second transition corresponds to the front of the reactive zone that travels along the column at constant velocity without changing its shape. In this last reaction zone, reaction occurs until the acetaldehyde has been completely consumed, since the amount of ethanol far exceeds acetaldehyde, and water displaces acetal from the stationary phase. In this reaction front, the acetaldehyde concentration front exhibits constant pattern behavior, since it propagates along the column at a constant velocity (at about 3.6×10^{-4} m/s $\cong 2.2$ cm/min, in Figure 7b) without changing its shape. Since water is being preferentially adsorbed by the resin while it is produced, the velocity of the water front is lower than that of the acetaldehyde front (at about 1.9 cm/min, in Figure 7d). The water front also exhibits constant pattern behavior. The acetal produced is immediately desorbed, increasing the acetal fluid concentration. After the reactive front zone, there are only acetal and ethanol in a separate front where acetal is eluting the ethanol initially present on the column. Since ethanol has more affinity to the resin than acetal, this front is dispersive, as shown in Figures 7a and 7c.

The two reaction zones can be better visualized if the calculated reaction-rate profiles inside the column at different times are plotted (Figure 8). The maximum reaction rate is observed at the entrance of the reactor; it then decreases

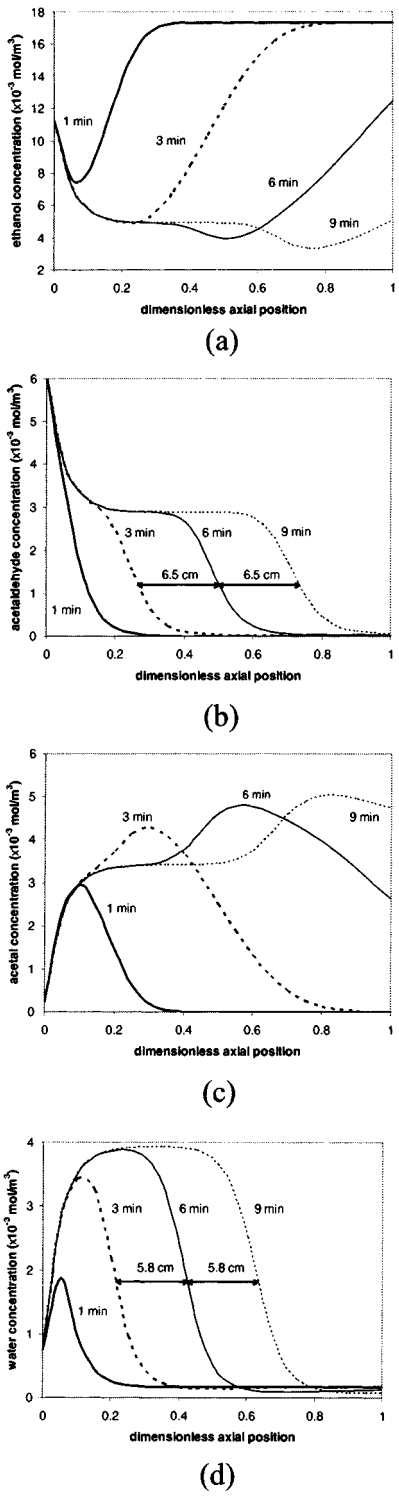

Figure 7. Internal concentration profiles of each species in fluid phase inside the column, at different times, during the reaction experiment of Figure 6: (a) ethanol; (b) acetaldehyde; (c) acetal; (d) water.

exponentially until $\zeta \cong 0.4$ (for $t = 12$ min), and this zone corresponds to the steady-state reaction zone. The second reaction zone moves along the column at constant velocity (at

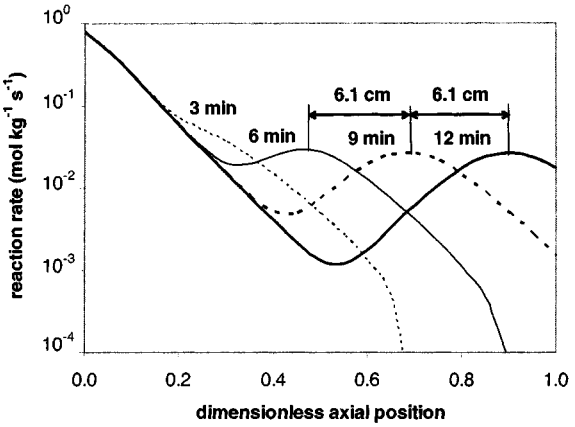

Figure 8. Calculated reaction-rate profiles inside the column for the experiment in Figure 6 at different times: 3 min (---); 6 min (——); 9 min (---); 12 min (——).

Table 5. Mass-Transfer Coefficients Estimated at 288 K, at the Inlet of the Column

Component	K_e ($\times 10^{+5}$ mol/s)	K_i ($\times 10^{+5}$ m/s)	K_L ($\times 10^{+5}$ m/s)
Ethanol	7.70/5.92	1.88/1.32	0.68/0.48
Acetaldehyde	7.80/5.98	1.92/1.33	0.68/0.50
Acetal	5.38/4.13	1.10/0.77	0.40/0.28
Water	12.3/9.48	3.80/2.65	1.30/0.95

*The feed is a mixture of ethanol and acetaldehyde at stoichiometric ratio and the flow rate is 2.4×10^{-7} m^3/s (14.5 mL/min): particle radius = 239/327 μm.

about 3.4×10^{-4} m/s $\cong$ 2 cm/min, in Figure 8) and travels

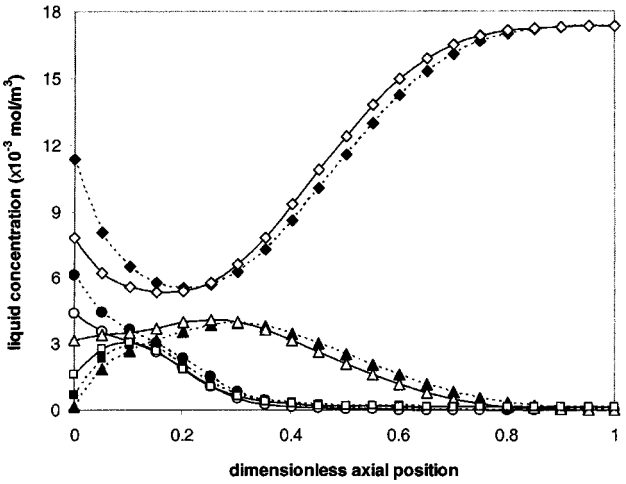

Figure 9. Calculated bulk concentration (dashed line with black symbol) and average particle concentration (continuous line with white symbol) profiles inside the column for the run show in Figure 6, at 3 min.

Model results: (◇) ethanol; (○) acetaldehyde; (△) acetal; (□) water.

together with the concentration fronts of acetaldehyde and water, whose velocities are 3.6×10^{-4} m/s ($\cong$ 2.2 cm/min) and 3.2×10^{-4} m/s ($\cong$ 1.9 cm/min), respectively, as shown in Figures 7b and 7d.

In order to assess the mass-transfer resistances, the values of the external, internal, and global-mass transfer coefficients are shown in Table 5, and it is thus concluded that the internal diffusion is the controlling mechanism. In Figure 9, the comparison between the bulk and the average particle concentrations is shown for the run in Figure 6, at time 3 min. At the entrance of the reactor, the ethanol and acetaldehyde are consumed by the reaction inside the particle, and since the mass transfer is not sufficiently high, the average particle concentration is lower than the bulk concentration. Two reaction experiments (Figure 10a and 10b), were achieved with a bigger pellet diameter ($d_p = 654$ μm) at a different flow rate and temperature, in order to validate the mass-transfer parameters estimation. The mass-transfer resistance in-

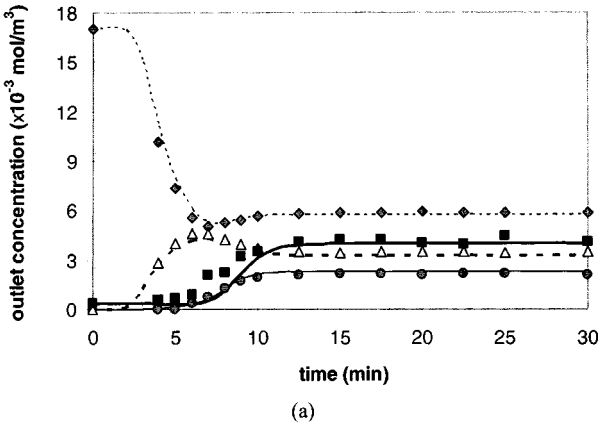

Figure 10. Concentration histories in a fixed-bed adsorptive reactor initially saturated with ethanol and then fed with ethanol and acetaldehyde, with particle diameter $d_p = 654$ μm.

Experimental conditions: (a) $Q = 3.4\times10^{-7}$ m^3/s (20.5 mL/min), $T = 288$ K, $C_{A0} = 12.3\times10^3$ mol/m^3, and $C_{B0} = 5.5\times10^3$ mol/m^3; (b) $Q = 2.3\times10^{-7}$ m^3/s (13.5 mL/min), $T = 283$ K, $C_{A0} = 12.2\times10^3$ mol/m^3 and $C_{B0} = 5.6\times10^3$ mol/m^3. Experimental data: (♦) ethanol; (●) acetaldehyde; (△) acetal; (■) water. Model results: (---) ethanol; (——) acetaldehyde; (---) acetal; (——) water.

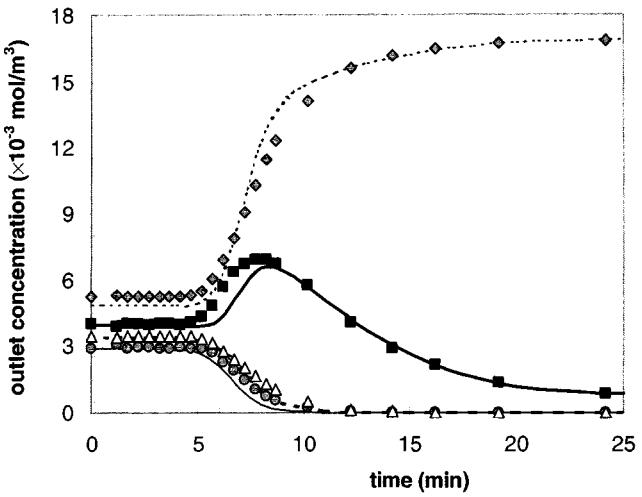

Figure 11. Concentration histories in the regeneration step of a fixed-bed adsorptive reactor.

The initial profiles in the bed are those at the final steady state of the run in Figure 6. Experimental conditions: $Q = 2.4\times10^{-7}$ m^3/s (14.5 mL/min), $C_{A0} = 17.0\times10^3$ mol/m^3, and $C_{B0} = 0.0\times10^3$ mol/m^3. Experimental data: (♦) ethanol; (●) acetaldehyde; (△) acetal; (■) water. Model results: (– – –) ethanol; (——) acetaldehyde; (– – –) acetal; (——) water.

creases (see Table 5), and the agreement between experimental and simulated results is quite good. The nonideality of the system is observed by analyzing the activities' coefficients calculated by the UNIFAC method. In a typical experiment, the activity coefficients ranges are [1.1–2.8] for ethanol, [1.3–2.1] for acetaldehyde, [0.6–2.7] for acetal, and [2.3–3.6] for water.

After the steady state is achieved, and before starting a new reaction experiment, it is necessary to regenerate the column. This step requires the use of a solvent to remove the adsorbed species. Ethanol was used as desorbent, although it is possible to use acetaldehyde to regenerate the resin. Figure 11 shows the regeneration step relative to the run represented in Figure 6. Acetal and acetaldehyde are the weakly adsorbed species and are the first to be desorbed. Water is strongly adsorbed and has much more affinity to the resin than ethanol, so large amounts of ethanol are needed to complete the water displacement. Again, in the regeneration step, agreement between model predictions and experimental results is satisfactory.

Conclusions

The dynamic behavior of a fixed-bed adsorptive reactor for the synthesis of diethylacetal, using an acid resin catalyst (Amberlyst 18), was studied.

The adsorption data were obtained by performing dynamic binary adsorption experiments, in the absence of reaction, at 288 K, in a laboratory-scale column. The adsorption parameters were optimized by minimizing the difference between the experimental and simulated stoichiometric times of the breakthrough curves. The internal mass-transfer coefficients were estimated by the Glueckauf approximating equation, and the Wilson and Geankoplis correlation was used to estimate the external mass-transfer coefficients.

A mathematical model for the adsorptive reactor was developed, including axial dispersion, external and internal mass-transfer resistances, and constant temperature; multicomponent Langmuir adsorption isotherms and reaction rate were measured in our laboratory. Model equations were solved by orthogonal collocation by finite elements, using the measured model parameters. The model was validated by comparing the experimental results obtained for the production and regeneration steps. Quite a good agreement between the model predictions and the experimental data was observed. This tool will be used in future work on the synthesis of diethylacetal in a simulated moving-bed adsorptive reactor.

Acknowledgment

V. Silva acknowledges financial support from Fundação para a Ciência e a Tecnologia (Research Fellowship: PRAXIS XXI/BD/13915/97). This work was carried out in the framework of the project CYTED IV.9—Production of Oxygenated Additives to Diesel from Ethanol. This article is based on a paper presented at NASCRE-1, Jan. 2001, Houston.

Notation

a = liquid-phase activity
C = liquid-phase concentration, mol/m^3
$\overline{C}_p$ = average liquid-phase concentration inside the particle, mol/m^3
C_T = total liquid-phase concentration, mol/m^3
d_p = particle diameter, m
Da = Damköhler number
D_{Am} = diffusion coefficient for a dilute solute A into a mixture, m^2/s
D_{ax} = axial dispersion, m^2/s
D_m = molecular diffusivity, m^2/s
k_i = internal mass-transfer coefficient, m/s
k_e = external mass-transfer coefficient, m/s
k_c = kinetic constant, mol/kg$_{res}$·s
K = Langmuir equilibrium parameter, m^3/mol
K_{eq} = equilibrium constant
K_I = adsorption constant in Eq. 6
K_L = global mass-transfer coefficient, m/s
K_L^* = number of mass-transfer units
L = bed length, m
Pe = Peclet number
q = solid-phase concentration in equilibrium with the fluid concentration inside the particle, mol/m$^3_{res}$
Q = adsorption capacity, mol/m$^3_{res}$
r_p = particle radius, m
$\Re^p$ = reaction rate relative to fluid concentration inside the particle, mol/kg$_{res}$·s
Re_p = Reynolds number relative to particle
r_p = particle radius, m
Sh_p = Sherwood number relative to particle
Sc = Schmidt number
t = time, s
t_{st} = stoichiometric time defined in Eq. 20, s
T = temperature, K
u = superficial velocity, m/s
V_{ml} = molar volume in the liquid phase, m^3/mol
x = liquid-phase molar fraction
z = axial coordinate, m

Greek letters

ϵ = bulk porosity
ϵ_p = pellet's porosity
γ = activity coefficient
μ = fluid viscosity, kg/m·s
ν = stoichiometric coefficient

ρ = liquid density, kg/m^3
ρ_b = bulk density, kg$_{res}$/m^3
θ = dimensionless time coordinate
τ = tortuosity
ζ = dimensionless axial coordinate

Subscripts and superscripts

i = relative to component i, ($i = A, B, C, D$)
F = relative to the feed
0 = relative to initial conditions
p = relative to particle

Literature Cited

Aizawa, T., H. Nakamura, K. Wakabayashi, T. Kudo, and H. Hasegawa, "Process for Producing Acetaldehyde Dimethylacetal," U.S. Patent No. 5,362,918 (1994).

Azevedo, D. C. S., and A. E. Rodrigues, "Design Methodology and Operation of a Simulated Moving Bed Reactor for the Inversion of Sucrose and Glucose-Fructose Separation," *Chem. Eng. J.*, **82**, 95 (2001).

Balzano, L., and M. Laborde, "Sintesis de Acetal (1,1-dietoxietano). Estudo Cinético," Simpósio Ibero-Americano de Catélise, Sociedade Portuguesa de Química, Porto, Portugal (2000).

Barker, P. E., G. Ganetsos, J. Ajongwen, and A. Akintoye, "Bioreaction-Separation on Continuous Chromatographic Systems," *Chem. Eng. J.*, **50**, B23 (1992).

Bramwyche, P. L., M. Mudgan, and H. M. Stanley, "Manufacture of Diethyl Acetal," U.S. Patent No. 2,519,540 (1950).

Capeletti, M. R., L. Balzano, G. De-la-Puente, M. Laborde, and U. Sedran, "Synthesis of Acetal (1,1-Dietoxyethane) from Ethanol and Acetaldehyde Over Acidic Catalysts," *Appl. Catal.*, **198**, L1 (2000).

Carta, G., "Simultaneous Reaction and Chromatography," *Chromatographic and Membrane Processes in Biotechnology*, C. A. Costa and J. S. Cabral, eds., Kluwer, Dordrecht, The Netherlands (1991).

Chung, S. F., and C. Y. Wen, "Longitudinal Dispersion of Liquid Flowing Through Fixed and Fluidized Beds," *AIChE J.*, **14**, 857 (1968).

Fredeslund, A., J. Gmehling, and P. Rasmussen, *Vapor-Liquid Equilibria Using UNIFAC — A Group Contribution Method*, Elsevier, Amsterdam (1977).

Glueckauf, E., "Theory of Chromatography," *Trans. Faraday Soc.*, **51**, 1540 (1955).

Higler, A., R. Krishna, and R. Taylor, "Nonequilibrium Modelling of Reactive Distillation: A Dusty Fluid Model for Heterogeneously Catalyzed Processes," *Ind. Eng. Chem. Res.*, **39**, 1596 (2000).

Iwasaki, H., M. Kitayama, and T. Onishi, "Process for Producing Acetals," EP Patent No. 771,779 (1996).

Kaufhold, M. M., and M. T. El-Chabawi, "Process for Preparing Acetaldehyde Diethyl Acetal," U.S. Patent No. 5,527,969 (1996).

Kawase, M., T. B. Suzuki, K. Inoue, K. Yoshimoto, and K. Hashimoto, "Increased Esterification Conversion by Application of the Simulated Moving-Bed Reactor," *Chem. Eng. Sci.*, **51**, 2971 (1996).

Kawase, M., K. Inoue, T. Araki, and K. Hashimoto, "The Simulated Moving-Bed Reactor for Production of Bisphenol A," *Catal. Today*, **48**, 1 (1999).

Kelly, J., S. Chapman, P. Brereton, A. Bertrand, C. Guillou, and R. Wittkowski, "Gas Chromatographic Determination of Volatile Congeners in Spirit Drinks: Interlaboratory Study," *J. AOAC Int.*, **82**, 1375 (1999).

Kohlpaintner, C., M. Schulte, J. Falbe, P. Lappe, and J. Weber, "Aldehydes, Aliphatic and Araliphatic," *Ullmann's Encyclopedia of Industrial Chemistry*, Wiley-VCH, Weinheim (1999).

Lode, F., M. Houmard, C. Migliorini, M. Mazzotti, and M. Morbidelli, "Continuous Reactive Chromatography," *Chem. Eng. Sci.*, **561**, 269 (2001).

Madsen, N. K., and R. F. Sincovec, "PDECOL, General Collocation Software for Partial Differential Equations [D3]," *ACM Trans. Math. Soft.*, **5**, 326 (1979).

Mazzotti, M., A. Kruglov, B. Neri, D. Gelosa, and M. Massimo, "A Continuous Chromatographic Reactor: SMBR," *Chem. Eng. Sci.*, **51**, 1827 (1996).

Mazzotti, M., B. Neri, D. Gelosa, and M. Massimo, "Dynamics of a Chromatographic Reactor: Esterification Catalyzed by Acidic Resins," *Ind. Eng. Chem. Res.*, **36**, 3163 (1997).

Morrison, R., and R. Boyd, *Organic Chemistry*, Allyn & Bacon, Boston (1983).

Pöpken, T., L. Götze, and J. Gmelhing, "Reaction Kinetics and Chemical Equilibrium of Homogeneously and Heterogeneously Catalyzed Acetic Acid Esterification with Methanol and Methyl Acetate Hydrolysis," *Ind. Eng. Chem. Res.*, **39**, 2601 (2000).

Reid, R. C., J. M. Prausnitz, and B. E. Poling, *The Properties of Gases and Liquids*, McGraw-Hill, New York (1987).

Ruthven, D. M., *Principles of Adsorption and Adsorption Processes*, Wiley, New York (1984).

Santacesaria, E., M. Massimo, A. Servida, G. Storti, and S. Carrà, "Separation of Xylenes on Y Zeolites. 2. Breakthrough Curves and Their Interpretation," *Ind. Eng. Chem. Process Des. Dev.*, **21**, 446 (1982).

Sardin, M., D. Schweich, and J. Villermaux, "Preparative Fixed-Bed Chromatographic Reactor," *Preparative and Production Scale Chromatography*, G. Ganetsos and P. E. Barker, eds., Dekker, New York (1993).

Silva, V. M. T. M., and A. E. Rodrigues, "Synthesis of Diethylacetal: Thermodynamic and Kinetic Studies," *Chem. Eng. Sci.*, **56**, 1255 (2001).

Sundmacher, K., and U. Hoffmann, "Development of a New Catalytic Distillation Process for Fuel Ethers via a Detailed Nonequilibrium Model," *Chem. Eng. Sci.*, **51**, 2359 (1996).

Teja, A. S., and P. Rice, "Generalized Corresponding States Method for the Viscosities of Liquid Mixtures," *Ind. Eng. Chem. Fundam.*, **20**, 77 (1981).

Thüner, L. P., I. Barnes, T. Maurer, C. G. Sauer, and K. H. Becker, "Kinetic Study of the Reaction of OH with a Series of Acetals at 298 ± 4 K," *Int. J. Chem. Kinet.*, **31**, 797 (1999).

Manuscript received June 20, 2001, and received Sept. 10, 2001.